Engineering with Computers
https://doi.org/10.1007/s00366-019-00814-0

ORIGINAL ARTICLE

Multi-objective optimization of stainless steel 304 tube laser forming process using GA

Mohammadali Keshtiara[1] · Sa'id Golabi[1] · Rasoul Tarkesh Esfahani[2]

Received: 29 September 2018 / Accepted: 22 June 2019
© Springer-Verlag London Ltd., part of Springer Nature 2019

Abstract
Laser forming is one of the most recent forming processes developed which uses a laser beam to induce a deliberate thermal stress on a workpiece to form a sheet metal. Accordingly, bending tubes using laser beam have attracted the attention of many engineers. In this paper, we studied the effects of various laser beam parameters on the tube bending process. To investigate the effects of all the parameters, we performed a large number of analyses and generated applicable tube laser bending data. We utilized Taguchi design of experiment method to manage the finite element simulation of the laser forming process. Subsequently, to have an easier, but more flexible and more complete laser forming data bank, we employed artificial neural networks to predict the required tube bending parameters for the proposed forming criteria. Finally, we used genetic algorithm programming to solve the multi-objective optimization with respect to the laser forming parameters. The objectives include maximum bending angle, minimum ovality, minimum thickening, and minimum forming energy consumption. The results from this study indicate that we can use applied data tables to find the optimum tube laser forming parameters. The outcome of the numerical experiments is consistent with the existing literature on the laser forming process.

Keywords Laser forming · Tube bending · Finite element · Multi-objective optimization · Genetic programming · Neural networks

1 Introduction

The idea of laser forming as a modern thermoforming process originates from a similar process of flame bending or line heating. Laser forming is a spring back-free and non-contact forming process achieved by introducing non-uniform thermal stress into the workpiece with a focused laser beam. In this process, forming mechanisms are determined by the temperature field, which depends on the geometry of the workpiece, laser power, laser spot diameter, scanning velocity, scanning path, and material properties. A number of mechanisms for the laser forming process have been suggested in the literature. These mechanisms mainly comprise the temperature gradient mechanism (TGM), the buckling mechanism (BM) and the upsetting mechanism (UM). The UM acts when the irradiated surface is large in comparison to the workpiece thickness; The laser beam diameter is equal to or larger than the material thickness; additionally, the velocity of beam scan is low, thereby, the whole cross section of the sheet will be heated such that the temperature gradient between the top surface and the bottom surface is small. Therefore, the induced thermal expansion will be hindered by the surrounding material. In addition, the geometry of this part is structurally stiff and does not allow the buckling to take place. Therefore, the irradiated zone will be shortened (and thickened) and the workpiece will be bent locally. Tube bending has many industrial applications. Because of the ability of laser forming to produce forms and curves that cannot be created through mechanical bending, this mechanism can be applied in different ways to a wide range of forming results. This promising approach for producing complex tube shapes can be applied in numerous products such as heat exchangers, boiler helical and spiral

✉ Sa'id Golabi
golabi-s@kashanu.ac.ir

Mohammadali Keshtiara
keshtiara.mohammadali@gmail.com

Rasoul Tarkesh Esfahani
r_tarkesh@pmc.iaun.ac.ir

[1] Department of Mechanical Engineering, Faculty of Engineering, University of Kashan, Kashan, Iran

[2] Department of Mechanical Engineering, Najafabad Branch, Islamic Azad University, Najafabad, Iran

Published online: 19 August 2019

coil systems, air conditioners, automobile exhaust systems, medical patient lifts, engines, refrigeration systems and many other types of custom tube bending. The laser forming of metal sheets has been extensively investigated in the literature. Laser bending of tubes and its related physical mechanisms are very complicated due to the large number of parameters involved in this process. Limited studies have been done in the field of laser tube bending compared to laser forming of metal sheets.

Li and Yao studied the mechanism of tube laser bending in more detail with the FEM software "ABAQUS" and experimental investigations. They explained the causes for various aspects of deformation characteristics such as wall thickness variation, ovality, protruded intrados, and bending radius. Other characteristics of laser bent tubes such as asymmetry of deformation and the ways of reducing the asymmetry were also examined. A closed-form expression for the bending angle was also proposed [1]. To identify the relationship between the bending angle and the processing parameters, Hao and Li established a new analytical model for tube bending angle. Their model presents an analytical expression of the bending angle as a function of the energy (laser power, absorption, scanning speed), geometric (tube diameter and wall thickness) and material properties (coefficient of thermal expansion, density, heat capacity, Young's modulus, yield stress) [2]. They also investigated the development of stress and strain during laser tube bending through thermal–mechanical finite element transient analysis and discussed the mechanism of laser tube bending based on simulation results [3]. Hsieh and Lin simulated the transient state of a thin metal tube under buckling with axial preloads due to a continuous wave CO_2 laser beam, and compared them with the measurements such as the elongation of the tube, the surface temperature and axial force taken in the experiments [4, 5]. Safdar et al. investigated the effects of various beam geometries on stress distribution and other useful parameters of laser tube bending with the FEM package ANSYS. The availability of laser beams with rectangular shape opens up the possibility of axial scanning in laser tube bending [6]. Compared to circumferential scanning scheme which needs multiple passes and is too time consuming, the axial scanning of a rectangular (or line) source can potentially generate sufficient bending in a single axial scan. Zhang et al. conducted a numerical study of the bending mechanism, bending characteristics, and suitable operating conditions of various schemes of axial scanning by a line source, and compared the results with circumferential scanning by a circular (or point) source [7]. Safdar et al. [8] used finite element modeling for the study of scanning schemes on tube bending angle. Guglielmotti et al. [9] studied the bending of slotted tubes as well as enlarging one tube end with circumferential scanning paths. Wang et al. presented a scanning path planning strategy based on laser tube characteristics. Their strategy involves a method for calculating the geometric curvature of the final shapely tubes. They considered both plane bending and three-dimensional bending and obtained a three-dimensional scanning path plan by combining the data in the two-dimensional planes. In addition, they carried out an experimental verification for bending straight tubes into a two-dimensional sinusoidal and a three-dimensional helical coil-shaped tube using their strategy of scanning path planning [10].

FEM is a powerful tool for investigating the laser forming process. However, to achieve good tube bending quality, the FEM procedure has to be performed several times with different combinations of laser forming process parameters. Unfortunately, it is very difficult to consider so many parameters for such a complex process. Taguchi method is a popular experimental design method for engineering and scientific studies based on orthogonal array experiments, which can be designed to control experiments via optimization. Gollo et al. employed the Taguchi method to find the parameters which significantly improve the bending process of laser sheet metal bending [11]. Unfortunately, FEM is not only very time consuming, but also requires finding optimum parameters to suggest a practical laser forming process. Therefore, there is a need for faster and more efficient methods to understand the relationship between the deformed shape and the laser forming parameters. Understanding such a relationship should predict the desired parameters in a timely manner.

Artificial neural networks (ANNs) have the ability to analyze data as a predictive tool. A trained ANN is a nonlinear function, capable of representing a complex relationship between the responses (output) and given parameter settings (input), and can help make accurate predictions about this relationship. Cheng and Lin used three supervised neural networks to estimate sheet metal bending angles formed by laser. Inputs for these neural networks included the laser forming parameters such as spot diameter, scan speed, laser power, and workpiece geometries including thickness and length of sheet metal workpiece [12]. Chen et al. [13] proposed an adaptive fuzzy neural network to predict the sheet metal bending deformation. Du and Wang proposed an improved BP network based on the Double Chains Quantum Genetic Algorithm (DCQGA). Their predicted model of laser bending angle based on their proposed BPN-DCQGA network was set up in the process of sheet metal laser bending [14]. Shen et al. [15] and Tarkesh Esfahani et al. [16] constructed models for sheet metal bending angle in laser forming using adaptive fuzzy logic, called an adaptive network fuzzy inference system (ANFIS). Maji et al. present neural networks and fuzzy logic-based methods used for developing the models of bending angle and conducting an inverse analysis of the laser forming process [17].

Imhan et al. investigated the laser tube forming using experimental, analytical modeling, and numerical simulations. They considered changes of material specification during the process due to the temperature rise and modified their analytical model accordingly. PSO algorithm was also used in their model to optimize the analytical and experimental results and reduce the mean absolute error [18]. Again, Imhan et al. used a high-power pulsed Nd–YAG laser to irradiate stainless steel 304 tubes and while also employing a motorized rotation stage with a computer controller to hold and rotate the tube. They carry out experiment investigations to improve the laser tube bending process by enhancing the absorption coefficient of the material and the mechanical formability using laser softening heat treatment [19].

Many parameters affect the quality of laser tube forming, including laser power, spot diameter, scanning velocity, laser path length, the number of scans, among other parameters. Therefore, in practical laser tube bending's test, it is required to determine laser forming parameters which result in optimal tube bending. In this area, only Guan et al. have focused on optimization and inverse analysis of tube laser bending. They integrated the finite element method simulation process with genetic programming and optimized the laser bending process of tubes based on different objective functions. They maximized two objective functions separately: bending angle after single laser scan and the fixed bending angle after single laser scan. Therefore, these objective functions for a single laser scan could be approached by means of matching laser forming parameters [20].

It is clear that in addition to the primary purpose of laser tube bending, i.e., producing bending, undesirable deformations such as wall thickness variation and ovality occur which can distance the bending from the ideal state. Unfortunately, the presence of such consequences is inevitable. Every time genetic programming is executed to search through single-objective optimizations of the previous studies, a new and different solution for the laser forming parameters is found, which in turn leads to different ovality values of wall thickening. Hence, any set of laser forming parameters found cannot be expressed as an optimal solution and is just one of the many possible answers for the genetic programming. However, if more than one objective is simultaneously considered for the laser forming, especially when these objectives compete with each other, attempting to optimize the whole set of objectives makes the optimization problem a multi-objective one. The purpose of this paper is to achieve the laser forming parameters for tube bending angle to have minimum ovality and wall thickening as well as minimum energy consumption. These objectives conflict and the conditions leading to an optimal value of one objective results in non-optimal values for the others.

Therefore, if a state is found so that no other state is preferable to it, this said state will have the quality of being Pareto optimal. In this paper, first, neural networks with the LMBP algorithm are used to develop the nonlinear relationship model between the laser forming parameters and the output responses on the experimental data. As such, data samples are required for training and testing the neural networks. In addition, thermo-mechanical FEM model of the laser tube bending with Taguchi design of experiments is used to collect the required data. Then a non-dominated Sorting Genetic Algorithm NSGA-II is applied to find the Pareto optimal set of the laser tube bending process. By sorting bending angles in different laser scanning passes and taking into account the laser forming parameters, a set of conditions are presented to the user which can produce the desired bending in the tube. The approach proposed in this paper is shown in Fig. 1. The NN and GA from MATLAB toolboxes are used to develop the required network model and to solve the global optimization in this work.

2 Laser tube bending

Laser bending of tubes is generally achieved through the upsetting mechanism and two kinds of scanning schemes: circumferential scanning and axial scanning. These scanning schemes are shown in Fig. 2. Circumferential scanning was carried out in the middle of the tube length for a prescribed scanning angle. Multiple scans at the same location are usually required to generate sufficient bending. Axial scanning scheme may involve a continuous point-source irradiation

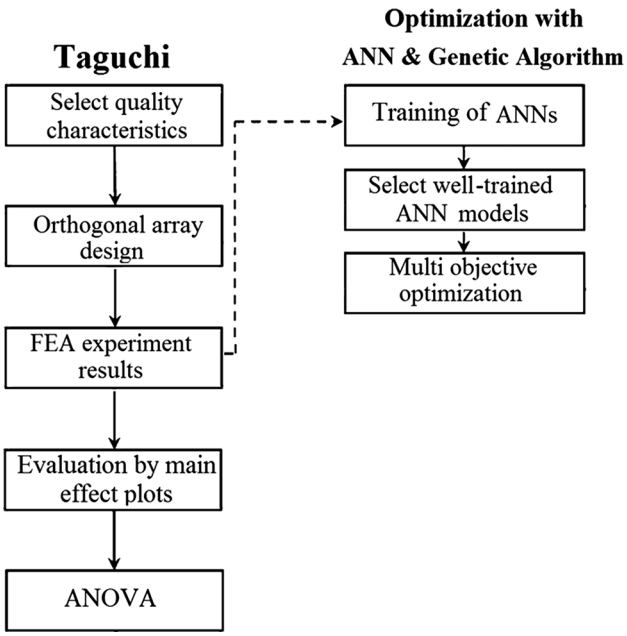

Fig. 1 Schematic diagram of the proposed approach

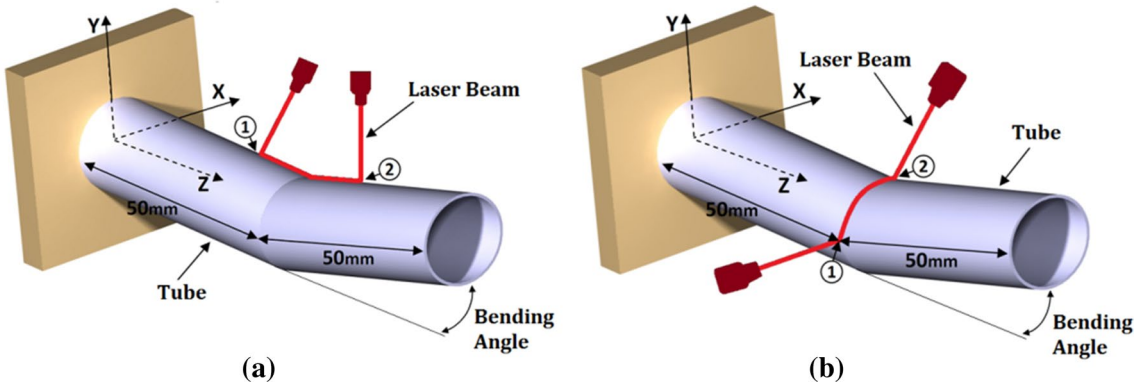

Fig. 2 Tube bending: **a** axial scanning, **b** circumferential scanning

of the tube along its axis. In this paper, only circumferential scanning scheme was investigated.

3 FEM model of laser tube bending

Laser tube bending process is modeled as a thermo-mechanical weakly coupled problem. It is assumed that the stress/deformation field depends on the temperature transient field. However, the temperature field can be found without knowledge of the stress/deformation response [21]. Therefore, due to the use of the laser beam source, the temperature transient field can be used as a thermal load to evaluate the stress–strain distribution and the final shape of the tube. Numerical simulations are performed using commercial finite element code ABAQUS. The material of the metal tube is AISI 304L. For finite element model, the following main assumptions have been made:

- During the entire laser tube bending process, no melting takes place.
- Heat generated through plastic deformation is negligible, compared to the energy input in laser bending.
- The tube material is isotropic and homogeneous.
- Melting is not involved in the plate during the forming process.
- Phase transformation is not accounted for in the simulation. Thus, both transformation strain and transformation plasticity are ignored.
- The effect of creep is negligible because there is no cyclic thermal load involved.
- The tube is initially stress free and strain free.

It is a primary condition to use the appropriate elements for finite element models to obtain the most accurate solution through the FE analysis. DC3D20 elements are used in thermal analysis in ABAQUS. Each DC3D20 element is a three-dimensional diffusion element with twenty nodes which allows for heat storage and heat conduction. They provide temperature output which can be used directly as input to equivalent stress elements [21].

The temperature-dependent properties of AISI 304L, thermal conductivity, specific heat, and density are important for accurate calculation of a temperature distribution, and are, therefore, used in the finite element model. The variations of these properties with temperature are given in Table 1. Initial temperature of the tube is 25 °C.

Table 1 Temperature-dependent thermal properties of AISI 304 [22]

Temperature (K)	Thermal conductivity k (W/m K)	Specific heat C_p (J/kg K)	Density ρ (kg/m^3)	Convection coefficient h (W/m^2)
300	14.7	477	7795	20
400	16.5	515	7245	–
600	19.0	557	6720	–
800	21.6	582	5290	–
1000	24.1	611	4310	–
1200	26.9	640	3315	–
1500	27.9	682	1856	–

Table 2 Mesh sensitivity analysis for circumferential scanning of tube based on maximum temperature

Test num.	Num. of elements through thickness	Total number of elements	Max. temp. at inner surface	Max. temp. at outer surface	Thermal analysis time (s)[a]
1	1	1186	698	1159	301
2	2	2408	700	1144	727
3	2	3850	702	1144	801
4	3	5202	703	1144	1246

[a]The solving time is calculated using parallel dual-core processor with base frequency of 2.67 GHz

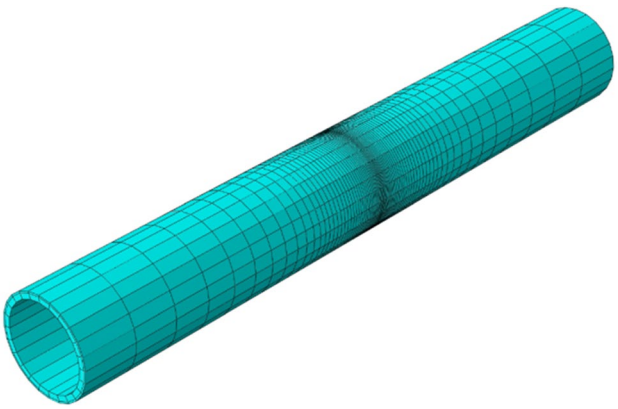

Fig. 3 Mesh model

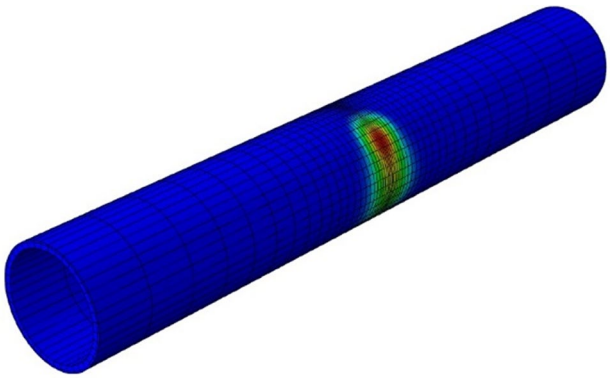

Fig. 4 The contour of the passage of laser beam

As shown in Table 2, the peak temperature at the midpoint of outer tube surface is not affected by increasing the number of elements over 2408. Therefore, the presence of two elements in the direction of thickness is sufficient for modeling.

According to Fig. 3, a biased mesh with ratio of 1:5 is used through the thickness and fine meshes are created in the region near the laser path due to the high heat flux involved in the portion, and other portions have coarse meshes. With this mesh pattern, both accurate results of simulation and reduction of computational time can be achieved. The same mesh is created for both thermal and mechanical analyses.

The thermal flux intensity on the tube surface caused by laser beam is modeled as a Gaussian distribution and is described as follows:

$$q_{(r)} = \frac{2\eta \cdot P}{\pi \cdot R^2} \exp\left(-\frac{2r^2}{R^2}\right), \tag{1}$$

where P is the laser power, R is the effective laser beam radius defined as the radius at which power density decreases to, and r is the distance from the center of the heat source and η is the laser absorption coefficient selected as 0.6. A user-defined subroutine is developed using FORTRAN in numerical simulation to define this Gaussian distribution.

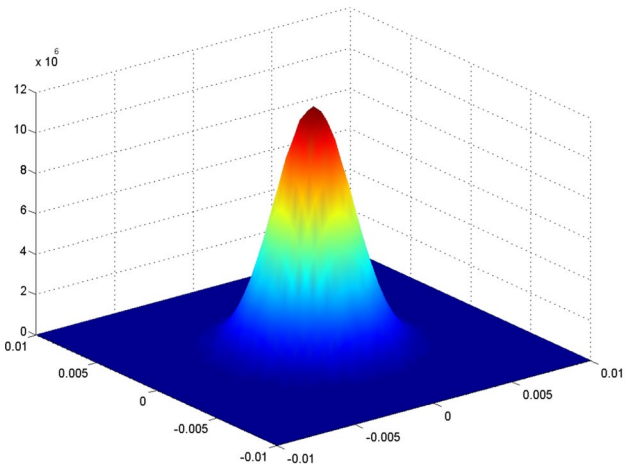

Fig. 5 Graphical schematic of laser heat source according to the Gaussian distribution Eq. 1. $P = 500$ W, $R = 3.5$ mm, $\eta = 0.6$

Heat losses from the tube surfaces to the surrounding areas take place by means of natural convection:

$$q_c = h\left(T_0 - T_\infty\right), \tag{2}$$

where h is the heat transfer coefficient and is set to 10.0. W/m^2, K is the surrounding temperature set to 25 °C. The contour of the passage of laser beam thermal flux (Fig. 4) has been illustrated by Gaussian distribution in ABAQUS software for the circumferential scanning in Fig. 5.

Table 3 Temperature-dependent elastic properties of AISI 304 [22]

Temperature (°C)	Coefficient of thermal expansion α (1/K)	Poisson's ratio (ν)	Elastic modulus E (GPa)
27	16 E−06	0.27	197
127	17 E−06	0.28	191
327	18 E−06	0.28	175
527	19 E−06	0.29	157
727	20 E−06	0.30	141
927	22 E−06	0.31	82
1227	23 E−06	0.32	16

Table 4 Temperature-dependent plastic properties of AISI 304 [23]

Temperature (°C)	Yield stress σ_y (MPa)	Plastic strain (MPa)
25	262	434
148	193	365
287	165	358
370	158	337
481	138	310
592	124	296
703	110	234
815	82	131
900	68	89
1000	62	62
1100	27	34

For developing the mechanical model in finite element, the material is modeled as thermo-elastic plastic with isotropic strain hardening. Material properties are assumed to be temperature dependent. The temperature-dependent Young's modulus and Poisson's ratio used for the elasticity model and temperature-dependent coefficients of thermal expansion for modeling the thermal strains are presented in Table 3.

Table 4 presents the yield stresses of AISI 304 steel at different temperatures. The missing data for some high temperatures are linearly extrapolated. In this simulation, the linear isotropic hardening is adopted and the behavior of the material after yielding is approximated to plastic strains.

All degrees of freedom at one end of the tube are restricted and the other surfaces are free. The element type in thermal stress analysis must be compatible with that in heat transfer analysis. A quadratic 20-node brick element, i.e., C3D20R, is used in the mechanical analysis because this kind of element has no shear locking and hourglass stiffness and is also suitable for bending deformation-dominated processes such as laser forming.

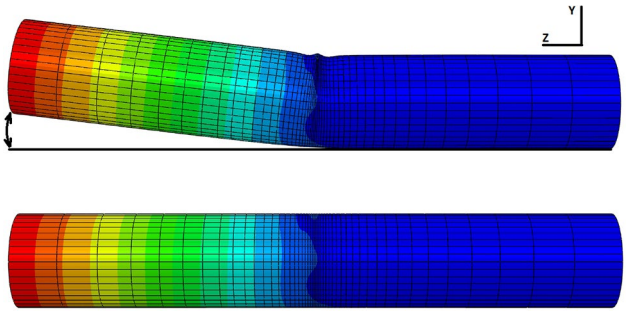

Fig. 6 Produced bending angle after circumferential scanning, power: 550 W, scanning speed: 2.5 rad/s, beam diameter: 7 mm, scanning path angle: 180°, tube outer diameter: 15.88 mm, wall thickness: 0.89 mm, length of tube: 100 mm

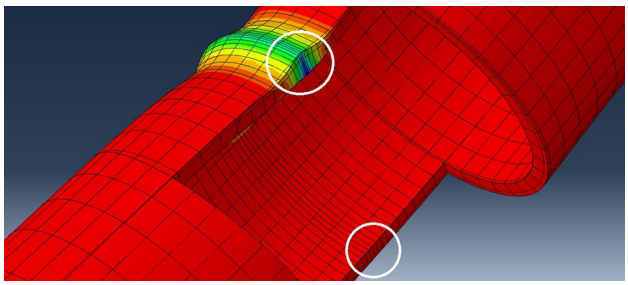

Fig. 7 Variation in the wall thickness in the scanning plane, thickening at the intrados and thinning at the extrados (magnification ×15)

4 Deformation characteristics

In this section, according to the simulated shape of a laser formed tube, the deformation characteristics considered in this paper are introduced. Figure 6 shows a bent tube angle after circumferential scanning in the middle and introduces the bending angle. Figure 7 shows that the material is shortened in the longitudinal direction. As a result, the thickness of the wall increases at the intrados. It can be seen that there is no appreciable thinning at the extrados.

Figure 8 shows the ovalization of a bent tube cross section. The ovalization is defined as follows:

$$\frac{D_{\max} - D_{\min}}{D_{\text{tube}}}, \tag{3}$$

where $D_{\max}$ and $D_{\min}$ are the maximum and minimum deformed diameters, respectively, and D_{tube} is the undeformed tube diameter [1].

In the present paper, the existing experimental results available in the literature [8] were used to validate the FEM simulation. Figure 9 shows a comparison of displacements in y-direction (instead of bending angle) for axial scanning scheme with the experimental results. It

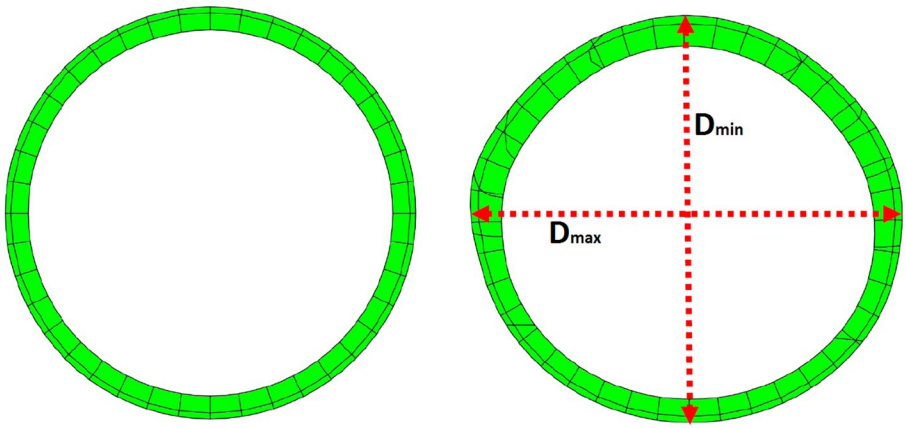

Fig. 8 Ovalization of the cross section (magnification ×15)

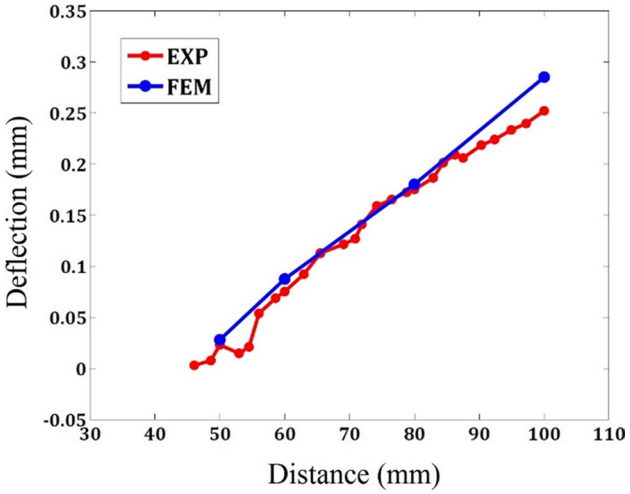

Fig. 9 FEM simulation of displacements in *y*-direction and its validation with experimental results of Ref. [8] for axial scanning scheme. Power: 200 W, scanning speed: 19.85 mm/s, beam diameter: 7 mm, axial scanning length: 20 mm, tube outer diameter: 14 mm, wall thickness: 1 mm, length of tube: 100 mm, number of scans: 4

can be seen that FEM simulation result is consistent with the experiment.

5 Design of experiments and parametric investigation of laser forming process

There are many factors affecting the laser tube forming process, but the current article focuses on a part of the process and geometrical factors, while the rest are considered as constant parameters.

To select a suitable array for the design of experiment, the number of the degrees of freedom required should be computed. Each of the four factors of laser beam (*P*), laser beam diameter (*D*), laser beam scan speed (*W*), and the rate of angular distance (CA) are studied at three levels.

Table 5 Effective factors in the process of circumferential laser tube bending and level changes for Taguchi method

Factors	Level changes		
	1	2	3
P			
Laser power (W)	300	400	550
D			
Laser beam diameter (mm)	6	7	8
W			
Laser beam velocity (rad/s)	1.5	2	2.5
CA			
Circumferential scanning angle (°)	90	120	180

Table 5 shows effective factors in the process of circumferential laser tube bending and considers different level changes.

Each factor has two degrees of freedom (DOF = *n*-1) where *n* is the number of the levels. The interference degree of freedom can be calculated by multiplying the degrees of freedom of the interfering factors. Due to the structural limitation of Taguchi method, evaluating the interference for all four factors is not possible in the Taguchi optimization; therefore, only the effects of the interference among the three factors of power, laser beam diameter, and scanning speed were taken into consideration. This means that the degrees of freedom for *P***D*, *P***W*, and *D***W* are all equal to 4 which is calculated in a similar manner (DOF = 2*2). The total degree of freedom for the four factors and the three interferences in this state equals to 20 (DOF = 3*4 + 4*2). The degree of freedom related to Taguchi orthogonal array should not be less than the degree of freedom of the whole experiment. Here, the most affordable selection is the L27 array with 13 columns and 27 rows. The result of the experimental design, along with the columns assigned to the interference effects among the factors in this state, can be seen in Table 6.

Table 6 Design of experiments of circumferential laser forming based on L27 orthogonal array with the effects of interference

Test num.	P	D	$P\times D$	–	W	$P\times w$	–	$D\times w$	CA	–	–	–	–
1	1	1	1	1	1	1	1	1	1	1	1	1	1
2	1	1	1	1	2	2	2	2	2	2	2	2	2
3	1	1	1	1	3	3	3	3	3	3	3	3	3
4	1	2	2	2	1	1	1	2	2	2	3	3	3
5	1	2	2	2	2	2	2	3	3	3	1	1	1
6	1	2	2	2	3	3	3	3	1	1	2	2	2
7	1	3	3	3	1	1	1	3	3	3	2	2	2
8	1	3	3	3	2	2	2	1	1	1	3	3	3
9	1	3	3	3	3	3	3	2	2	2	1	1	1
10	2	1	2	3	1	2	3	1	2	3	1	2	3
11	2	1	2	3	2	3	1	2	3	1	2	3	1
12	2	1	2	3	3	1	2	3	1	2	3	1	2
13	2	2	3	1	1	2	3	2	3	1	3	1	2
14	2	2	3	1	2	3	1	3	1	2	1	2	3
15	2	2	3	1	3	1	2	1	2	3	2	3	1
16	2	3	1	2	1	2	3	3	1	2	2	3	1
17	2	3	1	2	2	3	1	1	2	3	3	1	2
18	2	3	1	2	3	1	2	2	3	1	1	2	3
19	3	1	3	2	1	3	2	1	3	2	1	3	2
20	3	1	3	2	2	1	3	2	1	3	2	1	3
21	3	1	3	2	3	2	1	3	1	1	3	2	1
22	3	2	1	3	1	3	2	2	1	3	3	2	1
23	3	2	1	3	2	1	3	3	2	1	1	3	2
24	3	2	1	3	3	2	1	1	3	2	2	1	3
25	3	3	2	1	1	3	2	3	2	1	2	1	3
26	3	3	2	1	2	1	3	1	3	2	3	2	1
27	3	3	2	1	3	2	1	2	1	3	1	3	2

It is worth mentioning that the number of the laser scan pulses in all the 27 experiments has been equal to 30. To observe the rate of changes in average quality index for different levels of the factors, a diagram showing the effects of each factor is employed. Here, we used MINITAB 16, which is a specialized software in the area of experiment design. Larger-the-better state is selected for optimizing the quality index of the cross-sectional bending angle of the tube represented by BA. For indexes such as the percentage of the ovality of the middle cross section, angular asymmetry in the main bend (AS), the percentage of an increase in the thickness of the bent tube intrados (IT), and the percentage of the reduction of the outer arc thickness of the bent tube (OT), the smaller-the-better state is selected. Due to lack of repetition for the experiments of finite element in this paper, the diagram of the effects is similar when using S/N ratio or average values. The manner of the effect of each factor on the quality index of BA can be observed in Fig. 10.

By increasing the power of the laser beam, the rate of the tube bending also increases. An increase in each factor of the laser beam diameter and the speed of the laser scan leads to a reduction in the rate of the final bending. It is also observed

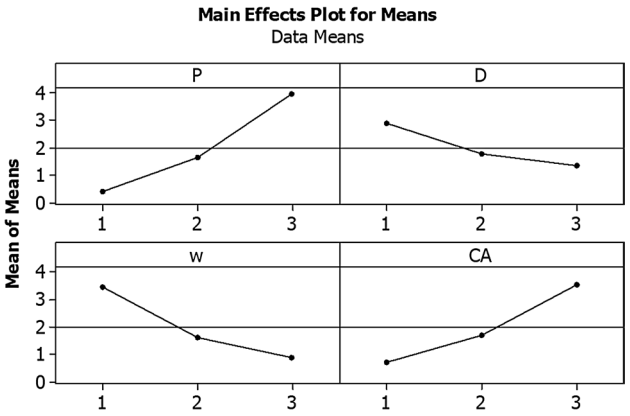

Fig. 10 Main effect plots for means of output bending angle

that by increasing the angular distance, laser scans the tube surface (CA), the final bending angle of the tube also shows an upward trend.

The analysis of variance (ANOVA) is a mathematical method that quantitatively expresses the relation between the factors and qualitative specifications intuitively obtained

Table 7 Results of ANOVA for the bending angle

Factor	Degree of freedom	Sum of square	Variance ratio	Percent contribution
P	2	58.78	11.77	30.64
D	2	11.63	2.33	6.06
w	2	31.84	6.37	16.6
CA	2	38.11	7.63	19.87
$P \times D$	4	9.82	0.98	5.12
$P \times w$	4	14.01	1.40	7.30
$D \times w$	4	12.58	1.26	6.6
Error	6	14.99	–	7.81
Total	26	191.78	–	100

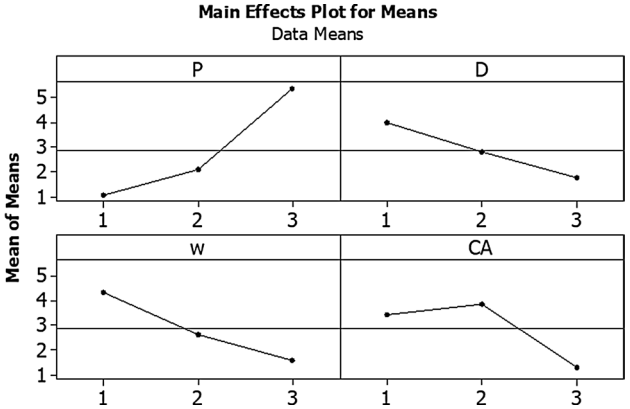

Fig. 11 Main effect plots for means of ovality%

from the diagrams of the main effects of the factors. Table 7 represents the results of ANOVA for bending angle. With regard to Table 7 and based on data of the percentage of participation, it is possible to rank the rate of effectiveness for each effective parameter in tube forming with the help of the laser beam. The power of the laser beam has the largest effect on the maximum rate of bending. Accordingly, the rate of the angular distance of the beam scan, laser scan speed, and laser beam diameter have the largest impacts on the change of the final shape. To observe the manner of the effectiveness of the parameters of laser forming process on the rate of ovality of the tube's middle cross section, diagram of effects on the quality index of (OV) is used which is shown in Fig. 11. As can be seen, an increase in the laser power results in an increase in the tube ovality. However, an increase in the parameters of the diameter of the laser beam, the speed of the laser scan, and the scanned circumferential distance leads to a decrease in the ovality of the middle cross section of the tube.

To increase the number of the training data for the neural network and to introduce the manner of the effectiveness

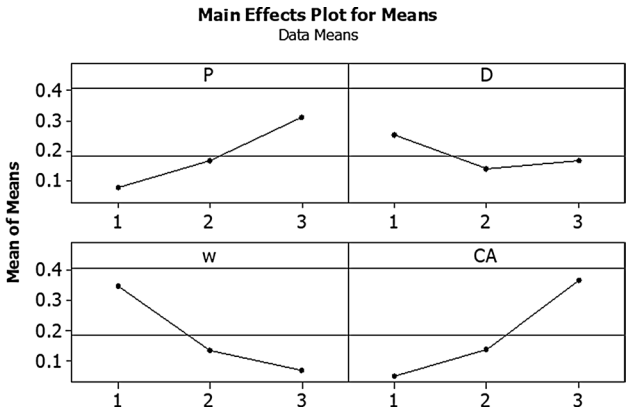

Fig. 12 Main effect plots for means of As

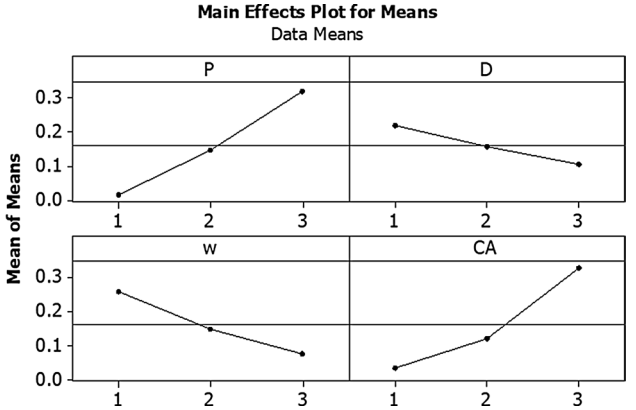

Fig. 13 Main effect plots for means of Ot

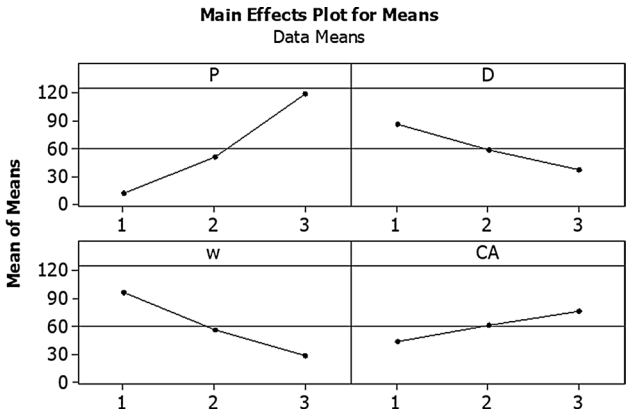

Fig. 14 Main effect plots for means of It

for other factors such as tube thickness and the number of laser beam pulses, a set of other orthogonal tests was also designed. The effects of the parameters of laser forming process on the quality indices of (As), (Ot), and (It) are shown in Figs. 12, 13 and 14, respectively.

Table 8 shows the factors under study and the levels of changes in new experiments. Here, the best selection is the L25 array from Table 9.

Figure 15 is obtained on the basis of the average tube thickness effect on the cross-sectional bent angle with regard to the results of the finite element experiments of L25 orthogonal design. It can be observed that an increase in thickness results in a decrease in the obtained bent angle.

Figure 16 shows the average effects of factors in Table 8 on the maximum surface temperature based on L25 orthogonal experiment design. It demonstrates an increasing in the power and angular distance of laser scan on the tube results in an increase in the temperature generated on the tube. Furthermore, increase in the speed of the laser beam and diameter of the tube results in decrease in the temperature on the tube surface. An increase in the tube thickness also has a descending effect on the maximum tube surface temperature.

6 Modeling of finite element result using neural networks

To create an efficient and automatic process, the required heating conditions for the scan path in laser forming process should be determined within a short time. Neural network is an efficient and suitable tool that provides immediate accessibility to the outputs for these processes. The architecture of the neural networks in MATLAB is designed in a manner that the finite element analysis output is used as the training data. Using the required processing parameters as the input, it is possible to employ neural networks for the prediction of tube deformations. Trained neural networks are able to predict the tube bending.

Table 8 Effective factors and level changes for the new orthogonal experiments

Control factors	Levels				
	1	2	3	4	5
P					
Laser power (W)	300	400	500	600	7300
D					
Laser beam diameter (mm)	4	5	6	8	11
t					
Tube thickness (mm)	0.889	1.067	1.245	1.651	2.108
NP					
Number of scan passes	20	1	5	2	10
w					
Velocity (rad/s)	1	1.5	2	2.5	3
CA					
Beam coverage (°)	90	100	120	150	180

Table 9 Design of experiments of circumferential laser forming based on L25 orthogonal array

Test num.	Control factors					
	P	D	T	N	V	C
1	1	1	1	1	1	1
2	1	2	2	2	2	2
3	1	3	3	3	3	3
4	1	4	4	4	4	4
5	1	5	5	5	5	5
6	2	1	2	3	4	5
7	2	2	3	4	5	1
8	2	3	4	5	1	2
9	2	4	5	1	2	3
10	2	5	1	2	3	4
11	3	1	3	5	2	4
12	3	2	4	1	3	5
13	3	3	5	2	4	1
14	3	4	1	3	5	2
15	3	5	2	4	1	3
16	4	1	4	2	5	3
17	4	2	5	3	1	4
18	4	3	1	4	2	5
19	4	4	2	5	3	1
20	4	5	3	1	4	2
21	5	1	5	4	3	2
22	5	2	1	5	4	3
23	5	3	2	1	5	4
24	5	4	3	2	1	5
25	5	5	4	3	2	1

The neural network input consists of geometrical and laser forming processes' parameters. Thickness is the geometrical parameter of the tube and the parameters of the laser forming process include power, laser diameter, scanning speed, number of scan pulses, and the angular distance of tube circumferential scan. The neural network

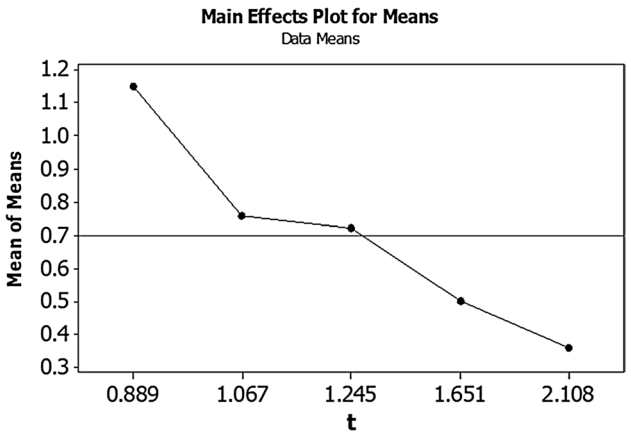

Fig. 15 The effect of thickness increasing on tube bending

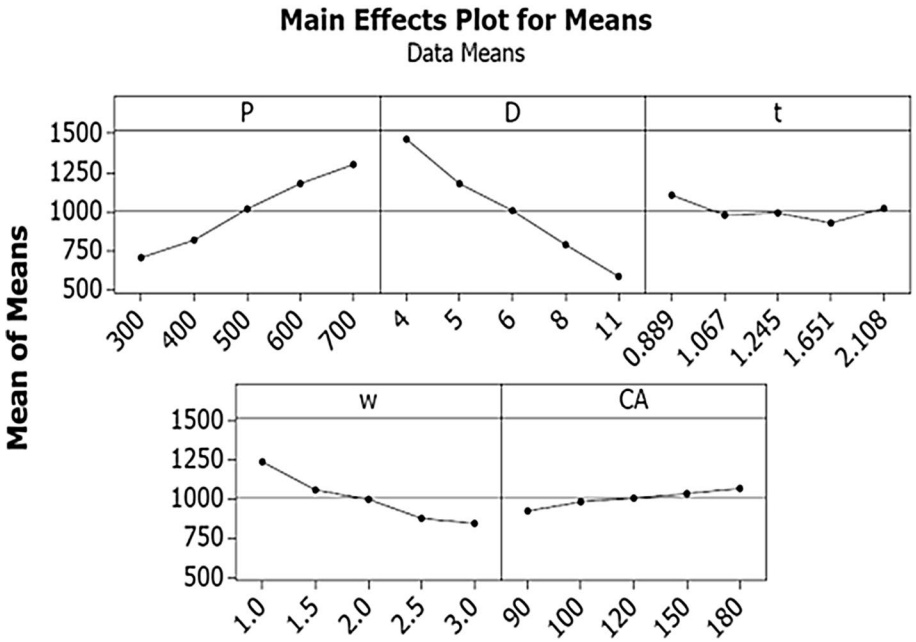

Fig. 16 Study the effects of laser forming geometric and process factors on maximum temperature of tube surface

also provides the maximum values for parameters of temperature on the laser scan path and tube deformations such as the rate of the main tube bending angle, the percentage rate of the ovality of the middle cross section in the scanning region, and the percentage of the increase of the intrados thickness at the tube middle cross section as its outputs. For each of these outputs, one separate neural network is trained. The tube external length and diameter are also considered constant at 100 mm and 15.88 mm, respectively.

The training data set for each network is the values of the data related to the design of the experiment. The data for scan numbers higher than one scan are saved in the finite element files. This data set, which includes a total of 210 experiments, is extracted for the training of the neural network. In other words, each of the input matrices for network training has a dimensionality of 6*210 and the training data matrix at the output of each network has a dimensionality of 1*210.

All the neural networks are designed on the basis of the neural network topology of proactive back-propagation of error. The raw architecture of neural networks is all constructed with the help of MATLAB software. The path with suitable potential efficiency has been selected for the selection of the final architecture for each network. Different combinations of the layers (single and double layers) with different numbers of neurons in each layer have been studied in this paper. To study each of these combinations, the weights and the biases of the networks have been reinitialized (assignment of value) multiple times. Supervision over the neural network has been performed with the help of five evaluation criteria in each initialization. These criteria are

- Network performance curve for training set, validation set, and experimental set.
- The sum of squared error between the network output and target vectors.
- Linear regression diagrams for the training set, the validation set, and the experimental set.
- The network outputs and target vectors with attention to statistically specific value (correlation coefficient).
- Comparison of the prediction and actual network performance against a number of unidentified inputs; R changes between zero and one and $R=1$ means full correlation among the data and $R=0$ means there is no correlation among the data.

The input data sets are presented to the network via sequential training and the training algorithm employed is the Levenberg–Marquardt algorithm. The generalization of some networks has been improved using self-adjustment method and others with the help of early stoppage method. The training stoppage of the network depends on different criteria such as the intensity of the gradients, the number of validation examinations, the minimum of the performance value, and the maximum of the number of the periods or iterations of training process.

In this paper, aside from the change in maximum number of iterations of the training process of the learning parameters of the Levenberg–Marquardt algorithm [24], the basis of the early stoppage method are also modified. In this state, 15%, 70%, and 15% of the input information have been allocated to the validation set, the training set, and the experimental set, respectively. The values of 1 mu, 1.5 mu, and 0.8 mu are allocated to fitting parameters, multiplier

coefficient, and reduction factor in this network, respectively. For the neural networks performing on the basis of self-adjustment method, 70% and 30% of the data are allocated to the network training and the experimental sets, respectively. The values of the fitting parameters, multiplier coefficient, and reduction factor in this network are set to 0.05 mu, 10 mu, and 0.1 mu, respectively. The trigger functions employed in the hidden layers for all the networks are the sigmoid hyperbolic tangent functions and a linear transfer function has been used for the output layer.

7 Rate of the tube cross-sectional bending parameter

The neural network related to this specification has an input layer and a multi-layer perceptron including two hidden layers and one output layer. The first hidden layer has eight neurons, the second hidden layer has one neuron and the output layer also has one neuron corresponding to its only output, i.e., the tube cross-sectional bending. Figure 17 shows that the network production outputs are properly conformed to the targeted vectors of the cross-sectional angle of the tube in the related classifications, i.e., the sections of training, experimental, validation, and the total data while the correlation coefficient approximates to one.

Figure 18 also shows that the training performance curves and the network test behave similarly and at the point of the network training stoppage, the test performance curve and the validation are close to each other. On the other hand, the mean squared error has also adopted the value of 3% for the validation set.

Table 10 also shows the network prediction results for the rate of the tube cross-sectional bending against a number of unidentified and random input data. Therefore, it seems that no over fitting has occurred. Data classification clearly shows that the generalization of this network has improved with the help of an early stoppage approach.

The neural networks are used to predict the maximum temperature and the percentage of the ovality of the tube cross section. The increase in tube thickness has similar effects to neural network process related to the tube bending. Therefore, the trained neural networks are able to predict the required outputs for laser forming. The output parameters

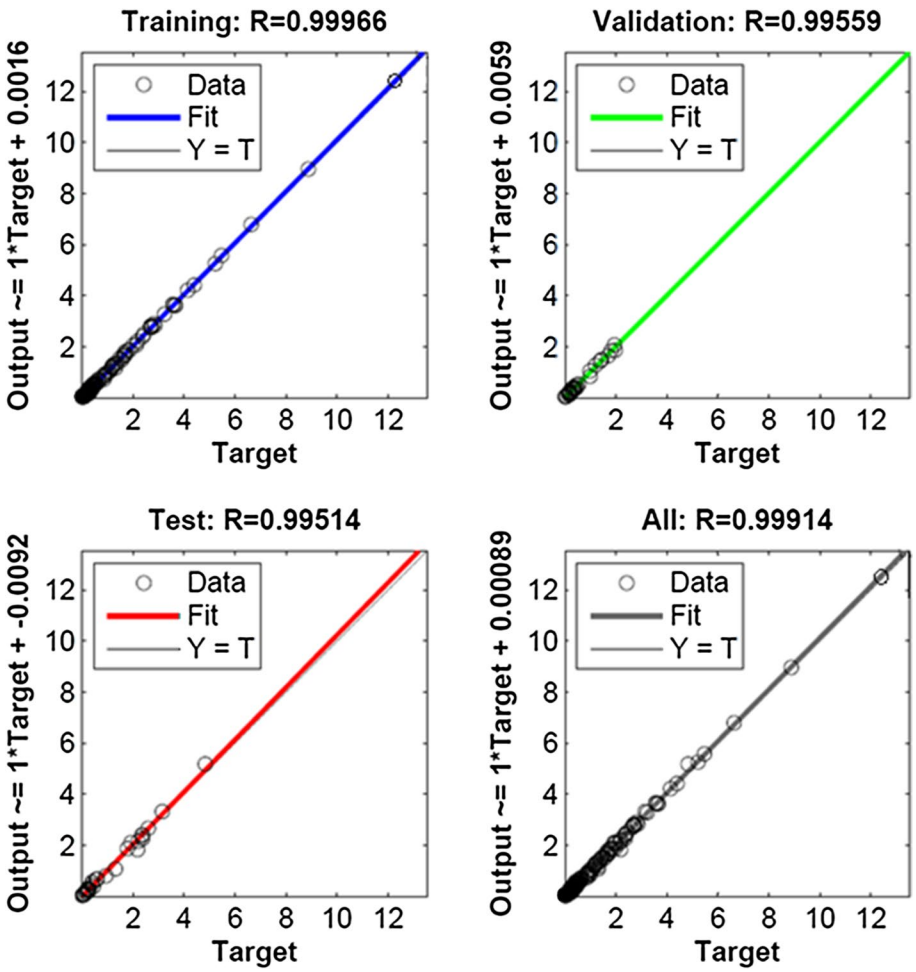

Fig. 17 Linear regression and the dependency coefficient for the training and experimental sets and the total of the network data between the output and target vectors for the tube cross-sectional bending

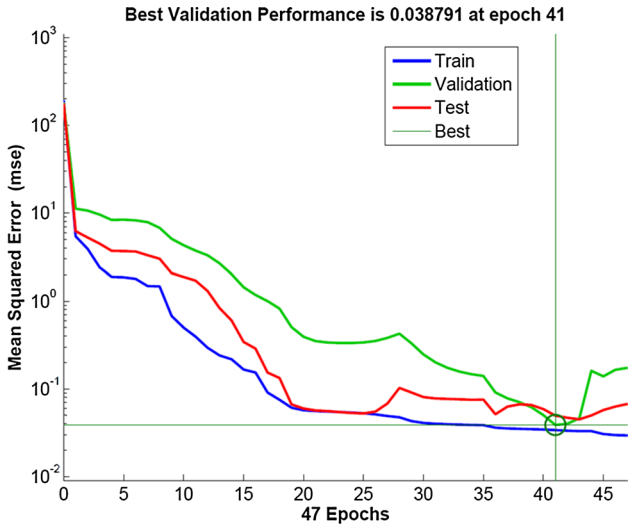

Fig. 18 The network performance curves (measurement on the basis the sum of the error squares) for the training and experimental set and validation of the tube cross-sectional bending

are related to the laser forming parameters in a complex and completely nonlinear manner. With the help of a suitable search algorithm, it is also possible to search the parametric space of the laser forming. Moreover, based on the indented conditions specified by the user, the laser forming parameters suitable for tube bending are obtained.

Table 11 shows the final neural network architecture for prediction of other necessary laser tube bending factors. Thus, trained neural networks are capable of predicting the required outputs of the laser forming process based on their complex and highly nonlinear relationship with the laser forming parameters.

8 Multi-objective optimization of laser tube bending

To enjoy the advantages of laser forming in the bending of tubes, it is necessary to adjust process parameters including the beam power, beam scan speed, laser beam effect diameter, and the distance covered by the laser beam to achieve optimal bending. The goal of this paper is to enable the user to bend the tube with specific and desired curvature and angle. The optimization of the bend produced at one cross section of the tube has been studied in this paper. Therefore, the user will decide to perform the laser scan process at n cross sections and produces the specific angle at each stage. Since the required angle at each cross section of the tube is identified, it is only sufficient to provide the parameters of tube laser forming process for the

Table 10 Neural network prediction for unknown data

Test		*P*	*D*	*W*	CA	NP	*T*	Max temp	BA	Ov	It
1	FEM 1	470	5	2.2	160	1	0.889	1147	0.176	1.633	4.813
	NN 1							1135	0.187	1.552	4.073
2	FEM 1	470	5	2.2	160	3	0.889	1149	0.450	6.500	12.333
	NN 1							1136	0.421	6.632	9.6662
3	FEM 1	470	5	2.2	160	5	0.899	1150	0.798	9.099	23.399
	NN 1							1136	0.785	10.102	18.951
4	FEM 1	680	6	1.7	180	1	2.108	1215	0.128	0.783	1.786
	NN 1							1202	0.139	0.692	1.801
5	FEM 1	680	6	1.7	180	4	2.108	1220	0.403	0.237	6.256
	NN 1							1203	0.380	0.204	4.974
6	FEM 1	680	6	1.5	180	8	2.108	1326	0.870	0.0731	14.532
	NN 1							1325	0.874	0.0704	14.691
7	FEM 1	600	5	1.5	180	8	1.651	1365	1.350	0.350	28.330
	NN 1							1365	1.366	0.356	28.149
8	FEM 1	550	5	1.5	150	6	1.245	1393	1.362	0.690	36.023
	NN 1							1393	1.354	0.598	34.597
9	FEM 1	600	9	1.4	150	2	0.889	1130	0.560	0.717	9.303
	NN 1							1133	0.564	0.603	9.633
10	FEM 1	500	4	2	180	1	0.889	1228	0.284	0.588	5.820
	NN 1							1467	0.261	0.561	5.771
11	FEM 1	500	4	2	180	3	0.889	1232	0.683	1.219	13.351
	NN 1							1468	0.983	1.108	13.489
	Average error of network with respect to the finite element							4.075	3.08	8.56	0.08

Table 11 Neural network topologies for the prediction of laser tube bending characteristics

Laser tube bending characteristics	Symbol	Topology
Maximum temperature of surface	Max Temp	6–8–2–1
Tube bending angle (°)	BA	6–8–1–1
Ovality percentage of tube at the scanning path plane	Ov	6–7–1–1
Increasing of thickness in the intrados	It	6–7–1–1

user (beam power, beam scan speed, the diameter of the laser beam effect, the distance covered by the laser beam, and the number of the scan passes of the laser beam). The main goal is the production of cross-sectional curvature in tube bending. Factors such as the rate of ovality of the circular cross section and an increase in the tube intrados thickness can also distance the bending from its the ideal state. The output of the problem presented in this section of the paper includes processing parameters of laser forming for which the most optimal bending angle is produced. The rate of ovality and the intrados thickness in the optimal state also tend toward the least possible values. The lowest energy consumption is also taken into consideration as much as possible. Furthermore, the suggested values for parameters of the laser forming process should not generate temperatures higher than the melting point of 304 steel on the tube. By sorting the bend angles at different scan passes along with the conditions of laser forming process for each bend angle, a set of the conditions for laser forming will be available to the user. Based on these conditions, it is possible to produce the intended bend in each tube with specific diameter and thickness. It is worth mentioning that the results are extracted for a fixed tube diameter. As it was specified, the abovementioned problem has three minimizations, one maximization and one constraint for keeping the temperature below the melting point. On the other hand, all these goals are also important for the problem. Therefore, the problem of finding the laser forming conditions should be regarded as a multi-objective optimization problem.

A multi-objective optimization problem (MOOP) deals with more than one objective function, which should be minimized or maximized. Most of the multi-objective optimization algorithms employ the concept of dominance. In this paper, the elitist non-dominated sorting genetic algorithm (NSGA-II) has been employed as the optimization tool for finding the Pareto optimal set. The values of the objective functions required

Table 12 Laser forming conditions for cross-sectional bending of a tube with a thickness of 0.889 mm

NP	*P* (w)	*D* (mm)	*W* (rad/s)	CA (°)	BA (°)	IT (%)	OV	*E* (J)
1	426	7.3	2.3	121	0.1	0.9	0.2	3167
1	473	7.0	1.8	124	0.2	2.9	0.2	4448
1	548	8.0	1.0	121	0.5	11.4	3.3	9053
2	547	7.1	1.3	142	0.6	16.3	2.5	8219
2	529	7.0	1.2	121	0.7	18.5	2.4	7629
3	552	7.7	1.2	113	0.7	19.6	3.3	7170
3	548	7.8	1.3	132	0.8	19.4	3.0	8009
3	563	7.4	1.2	155	1.2	23.7	1.3	9916
4	524	6.9	1.1	113	1.3	32.7	1.3	7425
4	530	7.2	1.1	122	1.5	33.9	3.5	8354
4	547	7.5	1.0	120	1.6	34.0	3.5	8831
5	543	8.2	1.2	143	1.7	33.3	2.3	9111
5	572	7.1	1.4	159	1.8	36.7	2.7	9152
5	579	7.9	1.1	146	2.2	43.8	2.4	10,563
6	562	7.3	1.2	164	2.7	50.3	2.6	10,489
6	572	6.5	1.3	160	2.7	53.9	3.4	9897
6	527	6.4	1.2	165	2.8	56.6	1.7	10,130
7	488	7.5	1.1	169	3.0	60.1	2.7	10,804
7	562	6.9	1.2	170	3.6	62.5	3.4	11,095
8	522	6.7	1.2	166	3.8	76.8	3.5	10,327
8	540	6.6	1.2	164	4.0	78.0	3.3	10,483
9	560	7.7	1.1	158	4.1	80.8	3.3	10,825
9	559	6.2	1.4	173	4.2	74.0	3.4	9839
9	560	7.6	1.1	175	5.0	82.1	2.4	12,322
10	578	7.2	1.1	175	5.9	90.6	2.9	12,166
10	582	7.2	1.1	177	6.1	90.1	2.7	12,474

by the genetic algorithm trained by the neural networks are computed and produced. The mathematical structure of this problem is as follows:

$$Max\,\alpha \text{ or } Min-\alpha, \tag{4}$$

$$Min\,Ov, \tag{5}$$

$$Min\,IT, \tag{6}$$

$$Min\,E, \tag{7}$$

where α is the cross-sectional bend angle produced in the tube, Oν is the percentage of ovality of the tube scanned cross section, IT is the percentage of increase in the tube intrados thickness, and E is the criterion for the measurement of the consumed energy.

The intervals in which the genetic algorithm is permitted to search for each one of the parameters of the laser forming process, i.e., laser beam power (P), laser beam diameter (D), laser beam scan speed (w), and the rate of angular distance (CA) are presented in the following equations. The number of the passes of the laser beam scan (N) can also change from 1 to 10. The units of P, D, V, and CA are Watt, mm, rad/s and deg, respectively,

$$300 \le P \le 700, \tag{8}$$

$$4 \le D \le 10, \tag{9}$$

$$1 \le w \le 2.5, \tag{10}$$

$$90 \le \text{CA} \le 180, \tag{11}$$

$$1 \le NP \le 10. \tag{12}$$

For the purpose of minimizing energy consumption and changing the search path of the genetic algorithm in the direction of energy issue, the energy term in Joules is defined using the following equation:

$$E = \frac{P \times l}{w}, \tag{13}$$

where w is the speed of the laser beam scan and l is the travel distance of the laser beam along the tube circumference. Ultimately, a maximum number of ten laser passes may be

Table 13 Laser forming conditions for cross-sectional bending of a tube with a thickness of 1.245 mm

NP	P (w)	D (mm)	W (rad/s)	CA (deg)	BA (deg)	IT (%)	OV	E (J)
1	446	7.2	2.2	109	0.1	0.8	0.1	3100
1	447	6.1	1.5	119	0.3	2.4	0.1	4961
1	580	6.8	1.1	142	0.5	10.0	0.1	10,747
2	517	7.5	1.0	126	0.6	8.6	0.4	8755
2	555	7.3	1.1	124	0.6	10.0	0.5	8424
2	582	7.3	1.0	147	0.7	14.4	0.2	11,486
3	563	6.7	1.2	128	0.8	19.2	0.2	8606
3	573	6.5	1.0	142	1.1	26.3	0.6	11,049
3	580	6.3	1.0	146	1.3	27.2	0.5	11,608
4	574	7.1	1.0	127	1.4	29.6	0.5	9847
4	571	6.0	1.0	142	1.6	36.6	0.5	10,769
4	588	6.6	1.0	162	1.7	29.2	0.4	12,757
5	563	6.2	1.2	165	1.9	32.0	0.4	11,155
5	572	6.0	1.0	169	2.3	37.7	0.4	12,797
6	564	6.2	1.1	159	2.4	44.5	0.6	11,231
6	564	6.4	1.1	171	2.5	41.1	0.4	12,302
6	564	6.1	1.1	169	2.6	43.7	0.5	12,183
7	555	6.0	1.2	167	2.8	48.2	0.4	11,081
7	567	5.7	1.2	163	3.0	52.6	0.4	11,123
7	562	5.8	1.1	167	3.1	53.1	0.4	11,641
8	545	5.8	1.0	148	3.5	74.4	0.5	11,050
8	588	6.3	1.0	169	4.4	65.9	0.5	13,661
8	591	6.4	1.0	174	4.5	62.9	0.5	14,076
9	586	6.6	1.0	169	4.7	72.1	0.5	13,668
9	592	6.4	1.0	171	5.0	71.8	0.5	13,753
10	590	6.0	1.0	162	5.5	86.5	0.8	13,114
10	587	6.0	1.0	168	5.7	83.7	0.6	13,443

used based on the conditions of laser forming for a tube with a diameter of 15.88 mm with several different thicknesses to achieve the desired bent angle.

Gamultiobj in MATLAB software is an algorithm which obtains the Pareto optimal answer for a multi-objective minimization problem based on elitist non-dominated sorting genetic algorithm (NSGA-II). Tables 12, 13, and 14 present the laser forming parameters required for the cross-sectional bending of the tube at different bending angles specified by the user. In each specific pass of the laser beam scan (1–10), the multi-objective optimization has been carried out based on the largest bending angle and the least rate of bending asymmetries and energy.

The NSGA-II algorithm calculates the required laser forming conditions for the objective functions and Pareto optimized values for each scan pass of the laser beam. Since there is no possibility to define a nonlinear constraint on optimization path for NSGA-II algorithm in MATLAB software, the laser forming parameters resulting in a temperature higher than the melting point of the tube were deleted initially. Among the remaining data of laser forming parameters, only the bending angles with a distance of 0.1° are selected. Undoubtedly, due to elimination of some of the data in the previous step, not all the angles are distanced by 0.1°. It is worth mentioning that the laser forming conditions might not be equal for a specific bending angle since other targets have generated different values. Therefore, they have no priority relative to each other in Pareto optimization issue. Accordingly, it is within the user's power to select the laser forming conditions in this state. For example, it is possible to select choices with less ovality percentage or with less increase in its intrados thickness; or in cases where the geometrical precision is not important for the user, but energy consumption is important, it is possible to select a state which consumes less energy. Furthermore, in the process of screening the laser forming results, the higher ranks of the laser scanning passes have been deleted. With regard to the functional structure of this algorithm, a limited number of the genetic algorithm results might not have been located on the optimal rows of Pareto. Therefore, re-monitoring is performed on the conditions of laser forming producing with similar cross-sectional bend angle and conditions in which the objective function is dominant are also deleted. As an example, in Table 12, conditions are provided for the case when user aims to bend a section of the tube with the length of 470 mm with thickness of 0.889 mm and a diameter of 15.88 mm according to Fig. 19 under a 45° angle and internal bending radius of 600 mm.

Table 14 Laser forming conditions for cross-sectional bending of a tube with a thickness of 2.108 mm

NP	*P* (w)	*D* (mm)	*W* (rad/s)	CA (deg)	BA	IT (%)	OV	*E* (J)
1	563	8.6	2.2	171	0.1	0.6	0.1	6004
2	547	7.7	1.3	136	0.2	1.1	0.1	8036
3	551	6.9	1.1	149	0.3	2.8	0.3	10,381
3	569	6.8	1.0	136	0.4	4.7	0.1	10,215
4	562	6.9	1.2	145	0.7	3.3	0.9	9820
4	592	5.7	1.0	164	1.0	13.5	0.1	13,317
4	593	5.5	1.0	172	1.1	15.0	0.1	14,033
5	568	6.1	1.0	154	1.2	10.6	0.8	11,959
5	568	5.9	1.0	174	1.3	13.5	0.2	13,372
6	575	6.4	1.1	158	1.5	10.8	1.1	11,665
6	574	5.7	1.1	162	1.6	14.1	0.7	11,886
6	575	5.3	1.0	166	1.8	21.0	0.3	12,874
7	567	5.4	1.1	157	1.9	20.1	0.6	11,715
7	572	6.0	1.0	165	1.9	19.8	1.4	12,633
7	573	5.4	1.0	163	2.1	25.7	1.6	12,809
8	588	5.4	1.1	162	2.2	25.2	1.8	12,040
8	587	5.3	1.1	165	2.3	27.5	1.3	12,396
8	586	5.3	1.0	165	2.4	31.2	1.7	12,813
9	580	5.4	1.1	167	2.5	27.6	1.1	12,153
9	581	5.3	1.1	173	2.7	35.8	1.2	13,088
9	580	5.0	1.1	174	2.8	38.4	1.5	13,128
10	576	5.1	1.1	175	3.0	39.5	1.4	12,837
10	577	5.0	1.0	175	3.3	48.7	1.9	13,541
10	577	4.8	1.0	176	3.4	51.6	1.7	13,657

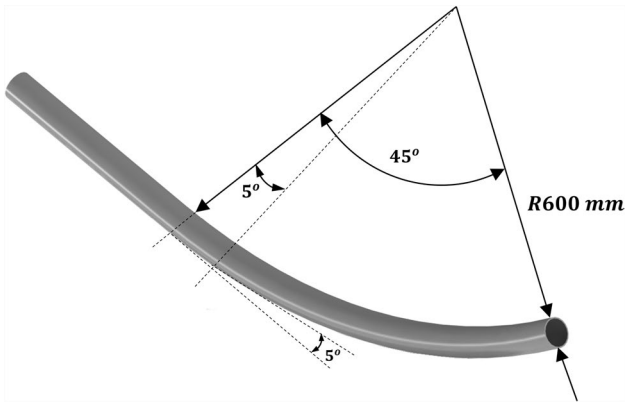

Fig. 19 Laser forming method of a stainless steel 304 tube (45° arc) using Table 12 data. The number of scan passes was set to 9 for this model

9 Conclusions and scope for future work

In this paper, the goal was to investigate the laser tube bending process and to extract applied data. Using ANOVA method, the influence of the tube bending parameters was studied. The results indicated that the laser beam power, the laser beam coverage, and the laser beam speed have the highest impacts on the tube bending. With the aid of the Pareto-based multi-objective genetic algorithm and neural networks, applied data tables were extracted to enable the users to bend a tube with a specific bending angle and curvature radius with the least ovality, the least thickening and the least forming energy consumption. As a potential future direction, this work can be further extended to provide complete data tables.

References

1. Li W, Yao YL (2001) Laser bending of tubes: mechanism, analysis, and prediction. J Manuf Sci Eng 123(4):674–681
2. Hao N, Li L (2003) An analytical model for laser tube bending. Appl Surf Sci 208:432–436
3. Hao N, Li L (2003) Finite element analysis of laser tube bending process. Appl Surf Sci 208:437–441
4. Hsieh H-S, Lin J (2005) Study of the buckling mechanism in laser tube forming. Opt Laser Technol 37(5):402–409
5. Hsieh H-S, Lin J (2005) Study of the buckling mechanism in laser tube forming with axial preloads. Int J Mach Tools Manuf 45(12–13):1368–1374
6. Safdar S, Li L, Sheikh M, Liu Z (2005) The effect of beam geometry on stress distribution in laser bending of tubes. Int Congress Appl Lasers Electro-Optics 1:106
7. Zhang J, Cheng P, Zhang W, Graham M, Jones J, Jones M, Yao YL (2006) Effects of scanning schemes on laser tube bending. J Manuf Sci Eng 128(1):20–33
8. Safdar S, Li L, Sheikh M, Liu Z (2007) Finite element simulation of laser tube bending: effect of scanning schemes on bending angle, distortions and stress distribution. Opt Laser Technol 39(6):1101–1110
9. Guglielmotti A, Quadrini F, Squeo E, Tagliaferri V (2008) Diode laser forming of stainless steel tubes. Int J Mater Form 1(1):1343–1346
10. Wang XY, Wang J, Wang L, Xu W, Guo D (2011) Scanning path planning in laser bending of tube based on curvature. Adv Mater Res Trans Tech Publ 264–265:6–11
11. Gollo MH, Mahdavian S, Naeini HM (2011) Statistical analysis of parameter effects on bending angle in laser forming process by pulsed Nd: YAG laser. Opt Laser Technol 43(3):475–482
12. Cheng P, Lin S (2000) Using neural networks to predict bending angle of sheet metal formed by laser. Int J Mach Tools Manuf 40(8):1185–1197
13. Chen D-J, Xiang Y-B, Wu S-C, Li M-Q (2002) Application of fuzzy neural network to laser bending process of sheet metal. Mater Sci Technol 18(6):677–680
14. Du Y, Wang X, Silvanus Jr (2010) Improved BP network to predict bending angle in the laser bending process for sheet metal. In: 2010 International Conference on intelligent system design and engineering application. IEEE, pp 839–843
15. Shen H, Shi Y, Yao Z, Hu J (2006) Fuzzy logic model for bending angle in laser forming. Mater Sci Technol 22(8):981–986
16. Esfahani RT, Zojaji Z (2016) Optimization of finite element model of laser forming in circular path using genetic algorithms and ANFIS. Soft Comput 20(5):2031–2045
17. Maji K, Pratihar DK, Nath A (2013) Analysis and synthesis of laser forming process using neural networks and neuro-fuzzy inference system. Soft Comput 17(5):849–865
18. Imhan KI, Baharudin B, Zakaria A, Ismail MISB, Alsabti NMH, Ahmad AK (2017) Investigation of material specifications changes during laser tube bending and its influence on the modification and optimization of analytical modeling. Opt Laser Technol 95:151–156
19. Imhan KI, Baharudin B, Zakaria A, Ismail MISB, Alsabti NMH, Ahmad AK (2018) Improve the material absorption of light and enhance the laser tube bending process utilizing laser softening heat treatment. Opt Laser Technol 99:15–18
20. Guan Y, Yuan G, Sun S, Zhao G (2013) Process simulation and optimization of laser tube bending. Int J Adv Manuf Technol 65(1–4):333–342
21. Hibbitt H, Karlsson B, Sorensen P (2011) Abaqus analysis user's manual version 6.10. Dassault Systèmes Simulia Corp, Providence
22. Hsieh H-S, Lin J (2004) Laser-induced vibration during pulsed laser forming. Opt Laser Technol 36(6):431–439
23. Scott P, Olson R, Bockbrader J, Wilson M, Gruen B, Morbitzer R, Yang Y, Williams C, Brust F, Fredette L (2005) The Battelle Integrity of Nuclear Piping (BINP) Program Final Report. No NUREG/CR-6837
24. Beale M, Hagan MT, Demuth HB (2011) Neural network toolbox, User's guide, MATLAB. The MathWorks Inc, Natick

Publisher's Note Springer Nature remains neutral with regard to jurisdictional claims in published maps and institutional affiliations.